Published in final edited form as:
*Sci Signal*. ; 2(88): ra53. doi:10.1126/scisignal.2000368.

# Tks5-dependent, Nox-mediated Generation of Reactive Oxygen Species is Necessary for Invadopodia Formation*

**Begoña Diaz***, **Gidon Shani***, **Ian Pass**, **Diana Anderson**, **Manuela Quintavalle**, and **Sara A. Courtneidge**#
Tumor Microenvironment Program, Burnham Institute for Medical Research, 10901 N Torrey Pines Road, La Jolla, CA 92037.

## Abstract

Invadopodia are actin-rich membrane protrusions of cancer cells which facilitate pericellular proteolysis and invasive behavior. We show here that reactive oxygen species (ROS) generated by the NADPH oxidase (Nox) system are necessary for invadopodia formation and function. The invadopodia protein Tks5 is structurally related to $p47^{phox}$, a Nox component in phagocytic cells. Knockdown of Tks5 reduces total ROS levels in cancer cells. Furthermore, Tks5 and $p22^{phox}$ can associate with each other, suggesting that Tks5 is part of the Nox complex. Tyrosine phosphorylation of Tks5 and Tks4, but not other Src substrates, is reduced by Nox inhibition. We propose that Tks5 facilitates the production of ROS necessary for invadopodia formation, and that in turn ROS modulates Tks5 tyrosine phosphorylation in a positive feedback loop.

## INTRODUCTION

Podosomes and invadopodia are related cellular structures present in cells with physiologically or pathologically invasive behaviors respectively (1–5). In 2-dimensional tissue culture systems, both structures are visualized as fine actin-rich protrusions of the ventral plasma membrane. A defining feature of both podosomes and invadopodia is the presence of pericellular proteolytic activity: matrix metalloproteases, ADAMs family proteases, cathepsins and the urokinase plasminogen activator system have all been found associated with these structures (6–10). The function of both podosomes and invadopodia is considered to be coordinated attachment to, and degradation of, the extracellular matrix (ECM), thus facilitating migration and invasion. Macrophages, endothelial cells, vascular smooth muscle cells and osteoclasts all form podosomes in response to activating stimuli. In contrast, many human cancer cells appear to contain invadopodia constitutively. Examples include breast cancers, melanoma, squamous cell carcinomas of the head and neck, and glioblastomas (6,11,12,9,13, 14). The ability of human cancer cells to form invadopodia has been correlated with their invasiveness, both in vitro and in vivo (15–18).

Reactive oxygen species (ROS), particularly superoxide and peroxide, can be produced in a number of ways (19). Some are produced in the mitochondria as a byproduct of the oxidative phosphorylation-dependent production of ATP (20), or in the endoplasmic reticulum as a consequence of protein misfolding (21). In cancer cells, mitochondrial dysfunction and



#Corresponding author: courtneidge@burnham.org, Phone: 858 646 3128.
*The order of these authors was chosen by lot

metabolic stress can lead to increased ROS production, with subsequent DNA damage and altered apoptotic responses (22–24). But ROS production can also be of physiological benefit. For example, high levels of ROS produced by activated phagocytic cells play an important role in host defense (25). And low levels of ROS are important for cell motility and proliferation of non-phagocytic cells (26–30). More recently, several reports have described ROS production in cancer cells, driven by tumorigenic signals such as activated Src or Ras, or overexpressed EGF or HGF receptors, and correlated it with survival, invasion and metastatic growth in vivo (31–34). Possible mechanisms by which ROS promote tumorigenesis include increased synthesis of matrix metalloproteases, amplification of signal transduction cascades by inhibition of protein tyrosine phosphatases (PTPases), and activation of protein kinase C (35–38).

One of the major cellular systems for the catalytic generation of ROS is the NADPH oxidase system (39–41). In phagocytes, this system comprises a membrane complex of gp91$^{phox}$ (also known as Nox2) and p22$^{phox}$, as well as cytosolic regulatory proteins, including p47$^{phox}$ (also known as NoxO2), p67$^{phox}$ (NoxA2) and the small GTPase Rac2. Cell activation, for example by bacteria, results in the phosphorylation of p47$^{phox}$, which relieves an autoinhibitory conformation, and allows the translocation of a complex including p47$^{phox}$, p67$^{phox}$ and Rac2 to the membrane to associate with Nox2. Rac, in concert with p67$^{phox}$, then catalyzes electron transfer from NADPH to FAD, with concomitant superoxide production. The expression of Nox2 is most prominent in phagocytic cells and the vasculature, and cannot explain ROS production in all cell types. More recently, homologous enzymes, Nox1, Nox3, Nox4 and the more distantly related Nox5, Duox1 and Duox2 were described, and their expression patterns elucidated (42–44). The p47$^{phox}$ homologue NoxO1, and the p67$^{phox}$ homologue NoxA1 were also described (45), although these proteins are not expressed in all cell types capable of generating ROS via NADPH oxidases. Nox1 has been implicated in ROS production in colonic epithelium, and is also expressed in colon cancer cell lines (46–50). Nox4 is more broadly expressed, and several cancers express this enzyme, particularly melanomas, glioblastomas and pancreatic adenocarcinomas (42,51–53).

Some years ago, we described the cloning and initial characterization of a new Src substrate we now call Tks5 (for tyrosine kinase substrate with 5 SH3 domains). Tks5 is a large adaptor or scaffolding protein, with no obvious catalytic activity (54). Instead it contains an amino terminal PX (phox homology) domain and five SH3 domains, as well as several polyproline motifs and two Src phosphorylation sites. Tks5 is cytoplasmic in normal cells, but localizes to invadopodia in Src-transformed mouse fibroblasts (Src-3T3) and human cancer cells (55). Reduction of Tks5 expression by shRNA results in the loss of invadopodia formation and invasive behavior in vitro (56), and reduced tumorigenicity in vivo (18). In addition, expression of Tks5, together with Src, in epithelial cells is sufficient to generate invadopodia (56). More recently, we characterized a close orthologue of Tks5, which we have called Tks4 because it consists of one PX and four SH3 domains. Tks4 is also required for functional invadopodia formation (57). We therefore consider that the Tks adaptor proteins play essential roles as invadopodia scaffold proteins.

A comparison of both the sequence and the overall topology of p47$^{phox}$ and Tks5 reveals that they have intriguing similarities (54,58,45). Each has an amino terminal PX domain followed by SH3 domains (2 in the case of p47$^{phox}$, and 5 in the case of Tks5). In addition, the first two SH3 domains of Tks5 have been predicted to form a tandem SH3 domain like those of p47$^{phox}$ (59). In the latter case, it is this tandem SH3 domain which mediates the association with a proline rich region (PRR) in p22$^{phox}$ (60). Both genes probably arose from the same primordial ancestor, and it is noteworthy that the simple chordate *Ciona intestinalis* has several Nox genes, but a single Tks-like gene consisting of a PX domain and 3 SH3 domains (45). The similarities between Tks5 and p47$^{phox}$, and the accumulating evidence of a role for ROS in

cancer invasion, led us to investigate whether ROS were required for invadopodia formation, and whether Tks5 was directly involved in ROS production. Our results are reported here.

## RESULTS

### ROS are required for, and localized to, invadopodia

We first asked if ROS are required for invadopodia formation and/or function. For these initial experiments, we chose to use a mouse fibrosarcoma model system, NIH-3T3 cells transformed with activated Src (referred to as Src-3T3), since these cells contain numerous invadopodia (also often referred to as podosomes in this cell background) arranged in characteristic rings or rosettes, and exhibit highly invasive behavior (56). These cells represent a highly relevant model system for the study of cell invasion, since several studies have now shown that both podosome formation in normal cells and invadopodia formation in human cancer cells are dependent on Src (1). When Src-3T3 cells were incubated with N-acetyl cysteine (NAC) a general anti-oxidant, we noticed a marked and dose-dependent loss of invadopodia (Figure 1A). Similar results were also obtained with the NADPH oxidase inhibitor diphenyleneiodonium chloride (DPI), but not with the lysyl oxidase inhibitor 3-aminopropionitrile (3-APN, Figure 1A). We also wanted to whether there was a requirement for NADPH oxidases for podosome formation. To this end, we cultured IC21 cells, a mouse peritoneal macrophage cell line known to elaborate podosomes (61), in the presence of DMSO or DPI. We found that DPI treatment markedly inhibited the formation of podosomes (Figure 1B), consistent with a role for ROS in the control of both podosome and invadopodia formation.

We noted that some punctate actin staining remained in the DPI-treated Src-3T3 cells. To determine the nature of these structures, we performed additional staining. First, a titration of phalloidin revealed a marked reduction in the actin concentration in these structures (Figure 1C). We also noted that they still contained Tks5 and cortactin, but not MT1-MMP (Supplementary Figure 1). Interestingly, in the DMSO treated cells, focal adhesion kinase (FAK) is localized to the rims of the rosettes, but is re-localized to focal contact-like structures and is not present in the actin puncta in DPI-treated cells (Figure 1D).

Since a prominent function of invadopodia is to coordinate the degradation of the extracellular matrix, we next plated Src-3T3 cells onto gelatin-coated coverslips, treated with DPI, and measured matrix degradation 6 hours later. The inhibitor significantly reduced degradation (Figure 2A), in a dose-dependent manner. Since these data suggested that ROS were required for invasive behavior, we also tested the effect of the inhibitors on the ability of Src-3T3 cells to move through matrigel-coated transwell chambers. Both NAC and DPI were effective, dose-dependent inhibitors in this assay (Figure 2B). Taken together, these data suggest that ROS are required for the invasive behavior of Src-3T3 cells. Since some ROS have short half-lives and therefore act in a spatially restricted manner, we also sought to determine the subcellular localization of the ROS in Src-3T3 cells. To this end, we incubated cells with the ROS sensor CM-DCF-DA, and visualized cells using both differential interference microscopy (DIC) and fluorescence microscopy. We noticed that while much of the ROS had a nuclear and/or perinuclear localization, some was clearly concentrated in the rosettes of invadopodia (Figure 2C), suggesting that it might be generated and/or function directly in these sites to facilitate invasive behavior.

### NADPH oxidases are involved in invadopodia formation

While DPI can inhibit several flavoproteins, one of its major effects is to inhibit the Nox family of NADPH oxidases. We therefore next tested whether Nox family enzymes are involved in invadopodia formation and function in Src-3T3 cells. Since all Nox family enzymes (with the possible exception of Nox5, which is not found in the mouse genome) require $p22^{phox}$ for

catalytic activity (62,63), we chose to first use siRNA to knockdown $p22^{phox}$. Figure 3A shows that cells transfected with a pool of $p22^{phox}$ siRNAs had significantly reduced numbers of invadopodia. Off target effects were ruled out by testing individual siRNAs: there was a complete correlation between degree of knockdown and extent of inhibition of invadopodia formation (Supplementary Figure 2). We also determined that gelatin degradation was inhibited by $p22^{phox}$ knockdown (Figure 3B). Since there is a paucity of affinity reagents capable of detecting endogenous levels of Nox family enzymes, particularly by immunoblotting, we next used RT-PCR analysis to determine which Nox enzymes are expressed in Src-3T3 cells. This analysis revealed mRNAs for Nox1, Nox3 and Nox4, but not Nox2 (Supplementary Table). Because there are reports in the literature (64,65) that the targeting of Nox4 to different subcellular compartments can modulate ROS-mediated signaling, we decided to focus on this isoform. By confocal microscopy, we noticed association of some Nox4 with invadopodia, as judged by its co-localization with F-actin (Figure 3C). And in keeping with a possible role for Nox4 in invasion, knockdown with a lentivirally-encoded shRNA sequence (Figure 3D) reduced both invadopodia formation and gelatin degradation. Similar effects on invadopodia formation were observed with a Nox4 siRNA (Supplementary Figure 3), ruling out off target effects. Note that since neither $p22^{phox}$ nor Nox4 antibodies are capable of recognizing cognate endogenous protein by immunoblotting, the degree of knockdown was quantitated by RT-PCR or qPCR in each case (Supplementary Figures 2 and 3).

Our next task was to determine the relevance of our findings in Src-3T3 cells to human cancer cells. Invadopodia have been found in many types of cancer cell, but are particularly well studied in melanoma, head-and-neck and breast cancer cells. Figure 4A shows that DPI inhibited invadopodia formation in a representative cell line from these cancer types, SCC61 (squamous cell carcinoma of the head-and-neck), and C8161.9 (melanoma). Furthermore, gelatin degradation was also inhibited by DPI treatment (Figure 4, panels A and B). Similar effects of DPI on invadopodia formation were obtained with the breast cancer line Bt549 and the melanoma RPMI-7951 (Figure 4C), although the small size of the structures and the presence of large numbers of actin fibers made further analysis of these cells of limited value.

To determine the possible role of NADPH oxidases in invadopodia formation in human cancer cells, we conducted a more detailed analysis of SCC61 cells and C8161.9 cells. We showed that siRNA-mediated $p22^{phox}$ knockdown in SCC61 both reduced invadopodia number and decreased gelatin degradation (Figure 5A, and Supplementary Figure 4). RT-PCR analysis of cancer cell lines suggests that SCC61 expresses Nox1, Nox2 and Nox4 (Supplementary Table). In contrast, and in keeping with the literature on melanoma cells, C8161.9 expresses predominantly Nox4 (51). We therefore used this cell line to probe both p22 and Nox4 function, and found that siRNA-mediated knockdown of either reduced invadopodia formation (Figure 5, panels B and C), concomitant with reduction of mRNA (Supplementary Figure 4). While outside the scope of the present study, in the future it will be interesting to dissect the roles of the individual Nox family members in invadopodia formation in the head-and-neck and breast cancer cells.

## Tks5 is required for ROS formation

When we first cloned and characterized Tks5 as a novel Src substrate (54), we noted its overall similarity to $p47^{phox}$. Both have amino terminal PX domains followed by SH3 domains. Furthermore, both the PX and the tandem SH3 domains have high degrees of similarity. We therefore hypothesized that Tks5, like $p47^{phox}$, is directly involved in ROS production, and tested our hypothesis using two different assay systems. In the first, we infected cells with scrambled or Tks5-specific shRNA encoding lentiviruses, incubated them with CM-DCF-DA to measure intracellular oxidants, and quantitated the data using a FACS machine (Figure 6A).

In the second, we measured oxidant production in control and Tks5 siRNA transfected Src-3T3 cells using a luminol-based chemiluminescence assay, which measures both intracellular and extracellular reactive oxygen (Figure 6B). In both cases, we observed a significant decrease in total cellular ROS upon Tks5 knockdown. Similar results were also obtained using the luminol assay on SCC61 cells (Figure 6C). Interestingly, in all cases the reduction in ROS levels achieved by reduction in Tks5 expression was the same as that achieved by Nox inhibition, either with DPI or with $p22^{phox}$ knockdown (see Supplementary Figure 4E for $p22^{phox}$ knockdown, and Figure 5, panels A–C for Tks5 protein levels). In the accompanying manuscript, Gianni et al demonstrate that Tks5 can act as an organizer protein for Nox1 and Nox3, but not Nox4. This result is in keeping with the literature, which suggests that Nox4 does not require organizer proteins (66). However, we found that the increase in ROS production in B16-F10 melanoma cells transfected with Nox4 and p22 requires Tks5 (Figure 6D and Supplementary Figure 5D). Taken together, these data suggest that the majority of Nox-dependent ROS production in Src-3T3 cells, and also in cancer cells, is dependent upon Tks5.

During ROS production in phagocytes, serine phosphorylation of carboxy terminal sequences of $p47^{phox}$ releases an intramolecular inhibitory interaction involving the tandem SH3 domains (67). This allows recruitment to membranes via association of the PX domain with phosphatidylinositol phospholipids, and the association of the tandem SH3 domains with $p22^{phox}$. Given the similarities between $p47^{phox}$ and the amino-terminal half of Tks5, we next tested whether Tks5 could also associate with $p22^{phox}$. To do this, we co-transfected 293T cells with $p22^{phox}$ along with tagged full length Tks5, as well as with a construct containing the first 390 amino acids of Tks5 (390) encompassing the PX domain and the first two SH3 domains (Figure 7A). We detected an association of $p22^{phox}$ with both forms of Tks5 (Figure 7B). These data suggest that the first two SH3 domains of Tks5 might be responsible for mediating the association. To explore this, we repeated the co-transfections, this time comparing wild-type Tks5 to constructs bearing point mutations in each SH3 domain independently, designated M1, M2, M3, M4 and M5 (Figure 7C). We detected a reduction in binding to the M1 mutant, and, to a lesser extent, to the M2 mutant. Next, to map the association site in $p22^{phox}$, we tested the P156Q mutant of $p22^{phox}$, which is in the proline-rich region which mediates the association with $p47^{phox}$ and NoxO1 SH3 domains. This is a naturally occurring mutation described in a person with chronic granulomatous disease, and has previously been reported to act as a dominant negative inhibitor of Nox-dependent ROS production (68). We observed a decreased association of this mutant with Tks5, when compared to the wild-type (Figure 7D). Finally, we measured the effects of combining the P156Q mutation of $p22^{phox}$ with mutation of both of the first two SH3 domains of Tks5 (Figure 7E). Each mutation alone reduced association, but the combined effect of mutations of both $p22^{phox}$ and Tks5 had an even greater effect. Taken together, these data suggest that Tks5 participates in Nox-mediated ROS production at least in part through association with $p22^{phox}$.

## The effect of invadopodia localized ROS

One effect of ROS, particularly hydrogen peroxide, is to transiently inhibit the catalytic activity of some tyrosine, dual specificity and lipid phosphatases, via conversion of the sulfhydryl group of the catalytic cysteine residue to sulfenic acid (69). Since many of the tyrosine phosphorylated proteins in invadopodia are Src substrates, we hypothesized that their phosphorylation might be ROS sensitive. To test this, we incubated Src-3T3 cells with DPI overnight, then lysed cells, immunoprecipitated several Src substrates, and immunoblotted with anti-phosphotyrosine antibodies (Figure 8A and Supplementary Figure 6). Remarkably, we found that most of the proteins we tested, including cortactin, Stat3, $p190^{RhoGAP}$ and Nck, were largely unaffected by DPI. In contrast, we observed a marked reduction in the phosphotyrosine content of Tks5 and Tks4. Since we have recently shown that the tyrosine phosphorylation of both Tks4 and

Tks5 is necessary for invadopodia formation [(57), and Stylli et al, in press) this result suggests that ROS might act locally to promote invadopodia formation by regulating protein tyrosine phosphatase activity. In keeping with this, we detected robust association of the tyrosine phosphatase PTP-PEST in invadopodia (Figure 8B). To determine whether PTP-PEST might play a role in invadopodia, we transfected Src-3T3 cells with a scrambled control or with a pool of siRNAs targeting PTP-PEST. It appeared that PTP-PEST knockdown increased the number of rosettes per cell, compared to control cells (Figure 8C). Rosette number can vary from cell to cell, but in our experience usually does not exceed 5 per cell. To evaluate rosette number in the knockdown cells specifically, we co-transfected cells with a fluorescent reporter oligo, and evaluated the phenotype of reporter positive cells. Of the 10 PTP-PEST siRNA transfected cells we evaluated, 8 had more than 20 invadopodia rosettes, compared to only 1 of 9 control cells. These data suggest that PTP-PEST may play a role in the formation of invadopodia and/or the control of rosette formation.

## DISCUSSION

We used chemical inhibition and siRNA-mediated $p22^{phox}$ knockdown to demonstrate that NADPH oxidase-generated ROS are required for the formation and function of invadopodia, both in mouse fibrosarcoma cells and in human cancer cells. This prompted us to determine the expression of Nox family members in cancer cells. We focused these analyses on Nox 1, 2 3 and 4. We did not analyze the expression of Nox5, Duox1 and Duox2, because these enzymes have been reported not to require $p22^{phox}$ for oxidant production. Src-3T3 cells express Nox1, Nox3, and Nox4, but not Nox2. For the human cancer cells, C8161.9 melanoma cells predominantly expressed Nox4, in keeping with previous reports on melanomas (51). In contrast, SCC61 head-and-neck cancer cells expressed Nox1, Nox2 and Nox4. We implicated Nox4 as playing an important role in Src-3T3 cells and C8161.9 cells. We found it expressed in invadopodia, and detected a reduction in invadopodia formation in Nox4 knockdown cells. In the future, we will determine which members of the Nox family are required in other cancer types. In the accompanying paper, Gianni et al show that in colon cancer cells, Nox1 is the most abundant NADPH oxidase, and is found localized to invadopodia in a Tks4-dependent manner. It is possible that different cell types require different Nox proteins, or that optimal invadopodia formation requires multiple Nox family members.

We found that Tks5 knockdown was sufficient to reduce total ROS levels markedly in Src-3T3 and SCC61 cells, suggesting that the Nox system is the predominant source of ROS in these cells. These results further suggest that even though we detected expression of the organizer NoxO1 in both cell types, it did not make a major contribution to ROS levels. It is possible that complexes involving NoxO1 in these cells are not active, or that Tks5 is at a much higher relative abundance and therefore plays the dominant role in oxidant production. It is also possible that invadopodia localization is critical for oxidant production, perhaps by recruitment of co-activators. In this regard, it may be important that the PX domain of Tks5, which is required both for functional invadopodia formation (56) and for oxidant production (Gianni et al, accompanying paper) is recruited to nascent sites of invadopodia formation via its association with PI 3,4-P2 (55,70). In contrast, the PX domain of NoxO1 associates preferentially with PI 4-P, PI 5-P, and PI 3,5-P2 and is found on several membranes (71). Regardless, our data implicate Tks5 directly in the Nox-mediated production of oxidants, which is in keeping with the findings of Gianni et al, who demonstrate that both Tks4 and Tks5 can act as Nox organizers in reconstitution assays (accompanying paper). We have found that the first two (tandem) SH3 domains of Tks5 can associate with p22. In other studies (Pass et al, manuscript in preparation), we have shown that Tks5 molecules mutated in either the first or second SH3 domain act as dominant negatives and prevent invadopodia formation in Src-3T3 cells. Taken together, these findings are consistent with a role for the Tks adaptor proteins targeting ROS production to invadopodia.

Nox4 appears to play an important role in Src-3T3 and C8161.9 cells, and the simplest model to account for its activity would be that a Nox4/p22 complex in association with Tks5 generates ROS in invadopodia. Yet it is thought that Nox4 does not require organizer proteins for oxidant production (66). Indeed, in the companion paper from Gianni et al, it is shown that 293 cell co-transfection of Nox4 with Tks4 or Tks5 does not increase Nox4-mediated ROS production. However, we have shown that transfection of Nox4 into melanoma cells increases total ROS levels in a Tks5-dependent manner. It is possible that Nox4 is more sensitive to a requirement for organizer proteins in certain cell backgrounds, or that Nox4 has a high affinity for the endogenous levels of Tks4 or Tks5 present in the 293 cells. Alternatively, the critical step might be Tks5-dependent localization to invadopodia, perhaps to bring Nox4 into proximity with as yet unidentified activator proteins. These possibilities will be explored in future studies.

It appears that the Nox-generated ROS might function directly in invadopodia. In particular, we determined that ROS inhibition resulted in the selective inhibition of tyrosine phosphorylation of Tks4 and Tks5, but not other Src substrates in invadopodia. We have recently shown that the tyrosine phosphorylation of these two proteins is required for functional invadopodia formation [(57), and Stylli et al, in press] suggesting that ROS acts in a positive feedback loop to promote invadopodia formation. In this model, Tks5 (and Tks4) are required for the focal generation of ROS, which promotes the tyrosine phosphorylation of these two proteins which in turn allows invadopodia formation. A seeming paradox is that we detected the PTPase PTP-PEST localized to the rosettes of invadopodia in Src-3T3 cells, and a previous report described the localization of PTP-PEST to podosomes of osteoclasts (72). Furthermore, we present evidence that knockdown of PTP-PEST appears to increase the number of rosettes of invadopodia in Src-3T3 cells. The control of PTP-PEST by NADPH oxidases is entirely in keeping with previous studies demonstrating its role in adhesion and migration, and its regulation by Nox in endothelial cells (73–75). But why should a structure that relies upon tyrosine phosphorylation contain a tyrosine phosphatase? Podosomes and invadopodia are dynamic structures, with a half-life of actin turnover in some cases of minutes. We speculate that invadopodia/podosome localization of PTPs would allow a cycle of transient activation and inactivation of their catalytic activity by ROS, and therefore a cycling of their substrate proteins between phosphorylated and non-phosphorylated forms. This in turn might contribute to the turnover of the entire structure. It will be important to determine whether tyrosine phosphatases other than PTP-PEST are also present in invadopodia, and how their activity might be spatially and temporally regulated. In addition, it is possible that lipid phosphatases can also be reversibly regulated by ROS, and at least one phosphoinositide 5-phosphatase, synaptojanin, has been localized to invadopodia (13). Other mechanisms by which ROS might function in invadopodia formation is by direct or indirect activation of PKC, of Src family kinases, of the MAPK signaling pathway, and/or of MMPs, all of which are also known to promote podosome/invadopodia formation and function (76,36,5,37,38).

While there are several reports in the literature on the effects of ROS on cancer cell growth, survival and invasion (36–38), fewer studies have focused directly on the possible roles of members of the NADPH oxidase family. However, one recent report demonstrates the upregulation of Nox4 in glioblastoma, and shows that reduction in expression enhances chemotherapy-induced apoptosis (77). Other studies describe similar findings in melanoma and pancreatic adenocarcinoma cells (51,53). Likewise, Nox1 over-expression has been correlated with Ras mutation in colorectal cancers, and is also an early event in the development of prostate cancer (48,49,78). The studies reported here link two key features of cancer cells that contribute to invasive behavior, the generation of reactive oxygen species by NADPH oxidases and the formation and function of invadopodia. The invadopodia scaffold protein Tks5, which is required for tumor cell invasion in vitro and in vivo (56,18) is a key player in this link. It participates directly in the focal generation of ROS, acts as a scaffold for the polymerization of the actin cytoskeleton, and coordinates the activity of pericellular proteases.

We show here that the formation of podosomes in macrophages is also dependent on ROS. In the future, it will be important to determine whether the concerted action of Tks adaptor proteins and NADPH oxidases also plays an important role in podosome formation and function, for example in osteoclasts, macrophages and vascular cells.

## MATERIALS AND METHODS

### Cell lines

Mouse Src-3T3 cells, C8161.9 human cancer melanoma cells and Bt549 human breast cancer cells were grown as previously described (56). SCC61 human head-and-neck carcinoma cells (a gift from A. Weaver) were grown in DMEM-high glucose (MediaTech) containing 20% FBS (Hyclone) and 0.4μg/ml of Hydrocortisone (Sigma) in 10% $CO_2$. IC-21 mouse macrophages were grown in RPMI (MediaTech) containing 10% FBS in 5% $CO_2$. B16-F10 mouse melanoma and HEK293T cells were grown in DMEM-high glucose containing 10% FBS and penicillin/streptomycin in 10% $CO_2$.

### DNA constructs

Overlapping PCR was used to generate constructs in which a single Flag epitope tag sequence was inserted downstream of the Tks5 or Tks5 deletion constructs. The vector used for the Flag Tks5 was pCMV-Tag 4B. For Myc tagged Tks5 and Tks5 point mutations we used the pRK5 plasmid. Point mutations in the different SH3 domains of Tks5 (M1=W118A, M2=W260A, M3=W441A, M4=W827A, M5=W1056A) were generated using QuikChange II site-directed mutagenesis (Stratagene). The $p22^{phox}$ wild-type and P156Q constructs were expressed from the pcDNA3.1 vector and were a generous gift from Ulla Knaus.

### Materials

We used the following antibodies: Anti-Nox4 (Abcam), anti-Tks5 (1737 serum), anti-$p22^{phox}$ (Santa Cruz), anti-Myc tag (Affinity BioReagents), anti-Stat3 (Santa Cruz), anti-PTP-PEST (a gift from T. Mustelin), anti-beta-Tubulin (Sigma), anti-Tks4, anti-cortactin, anti-phosphotyrosine, anti-RhoGAP p190, anti-Nck, anti-FAK, anti-MT1-MMP (all from Millipore). Anti-FlagM2 affinity gel was from Sigma. AlexaFluor488 and AlexaFluor568-conjugated phalloidin, AlexaFluor568-streptavidin and Oregon green-labeled gelatin were from Invitrogen. Biotin-anti-rabbit IgG was from Jackson Immuno-Research. AlexaFluor488 and AlexaFluor680 anti-Mouse and anti-Rabbit IgG were from Invitrogen. Growth factor reduced Matrigel invasion chambers and control inserts were from BD. Diphenyleneiodonium Chloride (DPI) was from Calbiochem and Luminol, HRP, 3-aminopropionitrile (APN) and N-Acetyl-L-cysteine (NAC) were from Sigma. Crystal violet was from EMD.

### RNAi experiments

Lentiviral shRNA constructs targeting mNox4 and mTks5 were from Sigma (TRCN0000076587 and TRCN0000105734 clones respectively). Lentiviral shRNA constructs targeting $hp22^{phox}$ were from Open Biosystems (clone TRCN0000064578). Lentiviruses were generated by the Burnham Institute for Medical Research Lentiviral Core Facility. The following siRNA constructs were purchased from Thermo Scientific: $mp22^{phox}$ (M-042497 pool and individual sequences), $hp22^{phox}$ (M-011020 pool and individual sequences), mNox4 (individual sequence J-058509-05), hNox4 (M-010194 pool), mTks5 (L-045361 pool), hTks5 (M-006657 pool), mPTP-PEST (M-042199 pool), and non-targeting siRNA#3 (D-001210-03-05) as a control. Reporter red fluorescent oligo (Block-iT) was purchased from Invitrogen. siRNA constructs were transfected using Lipofectamine 2000 (Invitrogen). Efficiency of RNA interference was monitored by RT-PCR or qPCR for $p22^{phox}$ and Nox4, and by immunoblotting for Tks5 and PTP-PEST.

### Immunofluorescence

Cells were fixed in 4% paraformaldehyde, blocked with 15% goat serum and incubated with anti-Nox4 (1:5000), anti-PTP-PEST (1:5000), anti-FAK (1:1000), anti-MT1-MMP(1:500), anti-Tks5 (1:1000), anti-Tks4 (1:1000) or anti-Cortactin (1:1000). Cells were washed and incubated with anti-mouse or anti-rabbit AlexaFluor 488 (1:500) or in the case of Nox4 and PTP-PEST with biotin anti-rabbit IgG (1:500) and streptavidin-AlexaFluor568 (1:500). F-actin was stained with AlexaFluor488 or 568-conjugated phalloidin (1:500). For the titration experiment in Figure 1, phalloidin was used at 1:500 to 1:16000. Nuclei were stained with Hoechst. Fluorescence microscopy images were obtained with a Zeiss Axioplan2 microscope equipped with a Zeiss Axiocam HRm CCD camera using Axiovision software. Confocal microscopy images were acquired with a Radiance 2100/AGR-3Q BioRad Multiphoton Laser Point Scanning Confocal Microscope equipped with Argon and Krypton lasers. Images were processed with Adobe Photoshop software.

### Invadopodia formation and function assays

Src-3T3 or IC21 cells growing on glass coverslips were treated for 6–8h with the indicated amounts of NAC or 3-APN or for 1h with the indicated amounts of DPI. Src-3T3 cells were transfected on glass coverslips, and processed for immunofluorescence at the indicated times. Human cancer cells were transfected at 50% confluency, re-plated 24h or 48h after transfection onto unlabeled gelatin-coated coverslips and processed for immunofluorescence at the indicated times. Quantification of invadopodia was performed on phalloidin stained samples on at least 15 randomly chosen fields representing around 150 total cells per experimental point. Src-3T3 cells containing at least one complete rosette of invadopodia were scored as positive, SCC61 cells containing at least 3 F-actin rich invadopodia were scored as positive, and C8161.9 cells containing F-actin rich invadopodia were scored as positive. Total cell numbers were calculated by scoring number or nuclei on the same samples. Quantification was expressed as percent of cells with invadopodia.

Invadopodia function assays were performed essentially as described (79) with some modifications. For DPI-treated Src-3T3, cells were plated on 0.2% labeled gelatin in 10% FBS-containing DMEM and allowed to attach for 1.5 hours before treatment. Cells were processed 5.5 h after treatment. For DPI treatment on human cancer cell lines, cells were plated on 0.2% labeled gelatin in 2.5% FBS-containing DMEM and allowed to attach for 2 hours before treatment with DPI. Cells were processed after 14–16h. For RNAi experiments, labeled gelatin was used at 1mg/ml and cells incubated in 1% FBS-containing DMEM. Src-3T3 cells were processed after 16–18h and human cells after 48h. Quantification of gelatin degradation activity was performed on at least 15 randomly chosen fields, representing a minimum of 200 total cells scored per experimental point. Quantification of the degradation area per field was performed using ImageJ software, and the percent of degraded area per field normalized to the number of cells on this field.

Motility and invasion assay was conducted as described before (56), except that 50–100,000 cells were used in each assay. NAC or DPI were added to the cells at the moment of plating on the upper chamber inset.

### Measurement of ROS

The luminol-based chemiluminescence assay was performed on attached cells. $10^4$ cells per well were plated on a 96-well tissue culture-treated white plastic plate (BD) and incubated O/N at 37°C. Cells growing on white plastic plates were washed twice with Hanks-balanced salt solution (HBSS) (Invitrogen) and incubated in HBSS containing 250μM Luminol and 1U Horseradish peroxidase (HRP). Chemiluminescence was immediately measured on a Veritas microplate luminometer (Turner Biosystems). For data normalization, a replica plate prepared

in parallel in a standard 96-well tissue culture plate was processed for crystal violet staining. Cells were washed with PBS and incubated with a solution containing 0.4% Crystal violet in 30% Methanol for 20min RT, washed 3 times with distilled water and allowed to dry. Dye was extracted with 1% SDS for 30min RT and optical density measured on a plate reader. ROS measurements were expressed as relative light units (RLU) normalized to optical density units (OD).

The 5-(and-6)-carboxy-2',7'-dichlorodihydrofluorescein diacetate (carboxy-$H_2$DCFDA) ROS fluorescent probe was used to detect endogenous ROS levels. For microscopy, $10^5$ cells were plated on glass-bottom 6-well plates (MatTek) and incubated O/N at 37°C. Cells were washed with HBSS and incubated with 25μM carboxy-$H_2$DCFDA (Invitrogen) in HBSS for 45min at 37°C in the dark. Cells were washed three times with HBSS, incubated in HBSS containing 1%FBS and imaged immediately. Imaging was performed using an Inverted TE300 Nikon Wide Field Fluorescence Microscope equipped with Nomarski (DIC) optics, ASI 2000 and Cooled Color CCD SPOT RT Camera (Diagnostic Instruments Inc.). Images were taken with neutral density filter and processed with Adobe Photoshop. For analysis of ROS levels by FACS, cells were washed 3 times with HBSS and incubated in HBSS containing carboxy-$H_2$DCFDA (25 μM) for 30 min at 37°C. Cultures were then harvested with trypsin/EDTA (1 min) and re-suspended in HBSS containing 10% FBS. Subsequently, cells were centrifuged for 5 min × 350g, re-suspended in 250 μl HBSS and analyzed. The flow cytometry data set was acquired using an unmodified FACSort (BD Biosciences, San Jose). DCF-DA fluorescence was detected from 515–545 nm.

### Tks5-p22$^{phox}$ association assay

HEK293T cells growing in 10cm dishes were transfected with 7–12μg of corresponding DNA constructs using lipofectamine 2000 according to the manufacturer's instructions, and harvested after 18h. Prior to lysis, cells were treated with cytochalasin D 1 μM for 1h, washed with PBS, trypsinized, and then lysed in ice cold B-buffer (30 mM Hepes, pH 7.6, 200 mM NaCl, 0.5 mM EDTA, 0.4% NP40), supplemented with standard protease inhibitors, 50mM beta-glycerophosphate and 100 μM sodium orthovanadate. Protein extracts were pre-cleared with protein A-PLUS-Agarose beads (Sigma) for 2 hours at 4°C. The pre-cleared extracts were incubated with beads that were blocked with 5% BSA. Lysates were subjected to immunoprecipitation with 20 μl anti-FLAG M2 affinity gel or 20 μl A-PLUS-Agarose incubated with 2 μl anti-Myc tag (9E10) for 2 hours at 4°C. Immunoprecipitates were subsequently washed 4 times with B-buffer containing 250 mM NaCl and 1 time with PBS. Proteins were eluted by heating the beads at 95°C in sample buffer, separated by SDS-PAGE and blotted with the specified antibodies.

### Immunoprecipitation

Subconfluent Src-3T3 cells were incubated O/N with 0.5μM DPI or the same volume of DMSO. 14–16h after treatment cells were lysed in CHAPS-based standard lysis buffer containing protease and phosphatase inhibitors for 45min at 4°C. 500–1000μg total protein were incubated for 1–2h 4°C with the corresponding antibody and 1h with protein-A or protein-G agarose beads. Product was analyzed by SDS-PAGE and standard immunoblotting conditions. Images were acquired using an infrared Odyssey Imager (LI-COR Biosciences). Processing and densitometry were performed using Adobe Photoshop.

## Supplementary Material

Refer to Web version on PubMed Central for supplementary material.

## REFERENCES


1. Linder S, Kopp P. Podosomes at a glance. J Cell Sci 2005;118:2079. [PubMed: 15890982]
2. Evans JG, Matsudaira P. Structure and dynamics of macrophage podosomes. Eur J Cell Biol 2006;85:145. [PubMed: 16546556]
3. Weaver AM. Invadopodia: specialized cell structures for cancer invasion. Clin Exp Metastasis 2006;23:97. [PubMed: 16830222]
4. Linder S. The matrix corroded: podosomes and invadopodia in extracellular matrix degradation. Trends Cell Biol 2007;17:107. [PubMed: 17275303]
5. Gimona M, Buccione R, Courtneidge SA, Linder S. Assembly and biological role of podosomes and invadopodia. Curr Opin Cell Biol 2008;20:235. [PubMed: 18337078]
6. Monsky WL, Lin CY, Aoyama A, Kelly T, Akiyama SK, Mueller SC, Chen WT. A potential marker protease of invasiveness, seprase, is localized on invadopodia of human malignant melanoma cells. Cancer Res 1994;54:5702. [PubMed: 7923219]
7. Nakahara H, Howard L, Thompson EW, Sato H, Seiki M, Yeh Y, Chen WT. Transmembrane/cytoplasmic domain-mediated membrane type 1-matrix metalloprotease docking to invadopodia is required for cell invasion. Proc Natl Acad Sci U S A 1997;94:7959. [PubMed: 9223295]
8. Chen WT, Wang JY. Specialized surface protrusions of invasive cells, invadopodia and lamellipodia, have differential MT1-MMP, MMP-2, and TIMP-2 localization. Ann N Y Acad Sci 1999;878:361. [PubMed: 10415741]
9. Artym VV, Kindzelskii AL, Chen WT, Petty HR. Molecular proximity of seprase and the urokinase-type plasminogen activator receptor on malignant melanoma cell membranes: dependence on beta1 integrins and the cytoskeleton. Carcinogenesis 2002;23:1593. [PubMed: 12376466]
10. Tu C, Ortega-Cava CF, Chen G, Fernandes ND, Cavallo-Medved D, Sloane BF, Band V, Band H. Lysosomal cathepsin B participates in the podosome-mediated extracellular matrix degradation and invasion via secreted lysosomes in v-Src fibroblasts. Cancer Res 2008;68:9147. [PubMed: 19010886]
11. Coopman PJ, Do MT, Thompson EW, Mueller SC. Phagocytosis of cross-linked gelatin matrix by human breast carcinoma cells correlates with their invasive capacity. Clin Cancer Res 1998;4:507. [PubMed: 9516943]
12. Kelly T, Yan Y, Osborne RL, Athota AB, Rozypal TL, Colclasure JC, Chu WS. Proteolysis of extracellular matrix by invadopodia facilitates human breast cancer cell invasion and is mediated by matrix metalloproteinases. Clin Exp Metastasis 1998;16:501. [PubMed: 9872598]
13. Chuang YY, Tran NL, Rusk N, Nakada M, Berens ME, Symons M. Role of synaptojanin 2 in glioma cell migration and invasion. Cancer Res 2004;64:8271. [PubMed: 15548694]
14. Bowden ET, Onikoyi E, Slack R, Myoui A, Yoneda T, Yamada KM, Mueller SC. Co-localization of cortactin and phosphotyrosine identifies active invadopodia in human breast cancer cells. Exp Cell Res 2006;312:1240. [PubMed: 16442522]
15. Tague SE, Muralidharan V, D'Souza-Schorey C. ADP-ribosylation factor 6 regulates tumor cell invasion through the activation of the MEK/ERK signaling pathway. Proc Natl Acad Sci U S A 2004;101:9671. [PubMed: 15210957]
16. Nam JM, Onodera Y, Mazaki Y, Miyoshi H, Hashimoto S, Sabe H. CIN85, a Cbl-interacting protein, is a component of AMAP1-mediated breast cancer invasion machinery. EMBO J 2007;26:647. [PubMed: 17255943]
17. Vishnubhotla R, Sun S, Huq J, Bulic M, Ramesh A, Guzman G, Cho M, Glover SC. ROCK-II mediates colon cancer invasion via regulation of MMP-2 and MMP-13 at the site of invadopodia as revealed by multiphoton imaging. Lab Invest 2007;87:1149. [PubMed: 17876296]
18. Blouw B, Seals DF, Pass I, Diaz B, Courtneidge SA. A role for the podosome/invadopodia scaffold protein Tks5 in tumor growth in vivo. Eur J Cell Biol 2008;87:555. [PubMed: 18417249]
19. Finkel T. Oxidant signals and oxidative stress. Curr Opin Cell Biol 2003;15:247. [PubMed: 12648682]
20. Starkov AA. The role of mitochondria in reactive oxygen species metabolism and signaling. Ann N Y Acad Sci 2008;1147:37. [PubMed: 19076429]
21. Gorlach A, Klappa P, Kietzmann T. The endoplasmic reticulum: folding, calcium homeostasis, signaling, and redox control. Antioxid Redox Signal 2006;8:1391. [PubMed: 16986999]

22. Kawanishi S, Hiraku Y. Oxidative and nitrative DNA damage as biomarker for carcinogenesis with special reference to inflammation. Antioxid Redox Signal 2006;8:1047. [PubMed: 16771694]
23. Federico A, Morgillo F, Tuccillo C, Ciardiello F, Loguercio C. Chronic inflammation and oxidative stress in human carcinogenesis. Int J Cancer 2007;121:2381. [PubMed: 17893868]
24. Mates JM, Segura JA, Alonso FJ, Marquez J. Intracellular redox status and oxidative stress: implications for cell proliferation, apoptosis, and carcinogenesis. Arch Toxicol 2008;82:273. [PubMed: 18443763]
25. Babior BM, Lambeth JD, Nauseef W. The neutrophil NADPH oxidase. Arch Biochem Biophys 2002;397:342. [PubMed: 11795892]
26. Abid MR, Kachra Z, Spokes KC, Aird WC. NADPH oxidase activity is required for endothelial cell proliferation and migration. FEBS Lett 2000;486:252. [PubMed: 11119713]
27. Devadas S, Zaritskaya L, Rhee SG, Oberley L, Williams MS. Discrete generation of superoxide and hydrogen peroxide by T cell receptor stimulation: selective regulation of mitogen-activated protein kinase activation and fas ligand expression. J Exp Med 2002;195:59. [PubMed: 11781366]
28. Ushio-Fukai M, Tang Y, Fukai T, Dikalov SI, Ma Y, Fujimoto M, Quinn MT, Pagano PJ, Johnson C, Alexander RW. Novel role of gp91(phox)-containing NAD(P)H oxidase in vascular endothelial growth factor-induced signaling and angiogenesis. Circ Res 2002;91:1160. [PubMed: 12480817]
29. Chiarugi P, Pani G, Giannoni E, Taddei L, Colavitti R, Raugei G, Symons M, Borrello S, Galeotti T, Ramponi G. Reactive oxygen species as essential mediators of cell adhesion: the oxidative inhibition of a FAK tyrosine phosphatase is required for cell adhesion. J Cell Biol 2003;161:933. [PubMed: 12796479]
30. ten Freyhaus H, Huntgeburth M, Wingler K, Schnitker J, Baumer AT, Vantler M, Bekhite MM, Wartenberg M, Sauer H, Rosenkranz S. Novel Nox inhibitor VAS2870 attenuates PDGF-dependent smooth muscle cell chemotaxis, but not proliferation. Cardiovasc Res 2006;71:331. [PubMed: 16545786]
31. Mitsushita J, Lambeth JD, Kamata T. The superoxide-generating oxidase Nox1 is functionally required for Ras oncogene transformation. Cancer Res 2004;64:3580. [PubMed: 15150115]
32. Ferraro D, Corso S, Fasano E, Panieri E, Santangelo R, Borrello S, Giordano S, Pani G, Galeotti T. Pro-metastatic signaling by c-Met through RAC-1 and reactive oxygen species (ROS). Oncogene 2006;25:3689. [PubMed: 16462764]
33. Gianni D, Bohl B, Courtneidge SA, Bokoch GM. The involvement of the tyrosine kinase c-Src in the regulation of reactive oxygen species generation mediated by NADPH oxidase-1. Mol Biol Cell 2008;19:2984. [PubMed: 18463161]
34. Binker MG, Binker-Cosen AA, Richards D, Oliver B, Cosen-Binker LI. EGF promotes invasion by PANC-1 cells through Rac1/ROS-dependent secretion and activation of MMP-2. Biochem Biophys Res Commun 2009;379:445. [PubMed: 19116140]
35. Tonks NK. Redox redux: revisiting PTPs and the control of cell signaling. Cell 2005;121:667. [PubMed: 15935753]
36. Wu WS. The signaling mechanism of ROS in tumor progression. Cancer Metastasis Rev 2006;25:695. [PubMed: 17160708]
37. Svineng G, Ravuri C, Rikardsen O, Huseby NE, Winberg JO. The role of reactive oxygen species in integrin and matrix metalloproteinase expression and function. Connect Tissue Res 2008;49:197. [PubMed: 18661342]
38. Wu WS, Wu JR, Hu CT. Signal cross talks for sustained MAPK activation and cell migration: the potential role of reactive oxygen species. Cancer Metastasis Rev 2008;27:303. [PubMed: 18299806]
39. Bokoch GM, Knaus UG. NADPH oxidases: not just for leukocytes anymore! Trends Biochem Sci 2003;28:502. [PubMed: 13678962]
40. Lambeth JD. NOX enzymes and the biology of reactive oxygen. Nat Rev Immunol 2004;4:181. [PubMed: 15039755]
41. Bedard K, Krause KH. The NOX family of ROS-generating NADPH oxidases: physiology and pathophysiology. Physiol Rev 2007;87:245. [PubMed: 17237347]
42. Cheng G, Cao Z, Xu X, van Meir EG, Lambeth JD. Homologs of gp91phox: cloning and tissue expression of Nox3, Nox4, and Nox5. Gene 2001;269:131. [PubMed: 11376945]

43. Kawahara T, Quinn MT, Lambeth JD. Molecular evolution of the reactive oxygen-generating NADPH oxidase (Nox/Duox) family of enzymes. BMC Evol Biol 2007;7:109. [PubMed: 17612411]
44. Lambeth JD, Kawahara T, Diebold B. Regulation of Nox and Duox enzymatic activity and expression. Free Radic Biol Med 2007;43:319. [PubMed: 17602947]
45. Kawahara T, Lambeth JD. Molecular evolution of Phox-related regulatory subunits for NADPH oxidase enzymes. BMC Evol Biol 2007;7:178. [PubMed: 17900370]
46. Geiszt M, Lekstrom K, Witta J, Leto TL. Proteins homologous to p47phox and p67phox support superoxide production by NAD(P)H oxidase 1 in colon epithelial cells. J Biol Chem 2003;278:20006. [PubMed: 12657628]
47. Fukuyama M, Rokutan K, Sano T, Miyake H, Shimada M, Tashiro S. Overexpression of a novel superoxide-producing enzyme, NADPH oxidase 1, in adenoma and well differentiated adenocarcinoma of the human colon. Cancer Lett 2005;221:97. [PubMed: 15797632]
48. Lim SD, Sun C, Lambeth JD, Marshall F, Amin M, Chung L, Petros JA, Arnold RS. Increased Nox1 and hydrogen peroxide in prostate cancer. Prostate 2005;62:200. [PubMed: 15389790]
49. Szanto I, Rubbia-Brandt L, Kiss P, Steger K, Banfi B, Kovari E, Herrmann F, Hadengue A, Krause KH. Expression of NOX1, a superoxide-generating NADPH oxidase, in colon cancer and inflammatory bowel disease. J Pathol 2005;207:164. [PubMed: 16086438]
50. Ushio-Fukai M, Nakamura Y. Reactive oxygen species and angiogenesis: NADPH oxidase as target for cancer therapy. Cancer Lett 2008;266:37. [PubMed: 18406051]
51. Brar SS, Kennedy TP, Sturrock AB, Huecksteadt TP, Quinn MT, Whorton AR, Hoidal JR. An NAD (P)H oxidase regulates growth and transcription in melanoma cells. Am J Physiol Cell Physiol 2002;282:C1212. [PubMed: 11997235]
52. Maranchie J, Zhan Y. Nox4 is critical for hypoxia-inducible factor 2-alpha transcriptional activity in von Hippel-Lindau-deficient renal cell carcinoma. Cancer Research 2005;65:9190. [PubMed: 16230378]
53. Mochizuki T, Furuta S, Mitsushita J, Shang WH, Ito M, Yokoo Y, Yamaura M, Ishizone S, Nakayama J, Konagai A, Hirose K, Kiyosawa K, Kamata T. Inhibition of NADPH oxidase 4 activates apoptosis via the AKT/apoptosis signal-regulating kinase 1 pathway in pancreatic cancer PANC-1 cells. Oncogene 2006;25:3699. [PubMed: 16532036]
54. Lock P, Abram CL, Gibson T, Courtneidge SA. A new method for isolating tyrosine kinase substrates used to identify fish, an SH3 and PX domain-containing protein, and Src substrate. Embo J 1998;17:4346. [PubMed: 9687503]
55. Abram CL, Seals DF, Pass I, Salinsky D, Maurer L, Roth TM, Courtneidge SA. The adaptor protein Fish associates with members of the ADAMs family and localizes to podosomes of Src-transformed cells. J Biol Chem 2003;278:16844. [PubMed: 12615925]
56. Seals DF, Azucena EF Jr, Pass I, Tesfay L, Gordon R, Woodrow M, Resau JH, Courtneidge SA. The adaptor protein Tks5/Fish is required for podosome formation and function, and for the protease-driven invasion of cancer cells. Cancer Cell 2005;7:155. [PubMed: 15710328]
57. Buschman MD, Bromann PA, Cejudo-Martin P, Wen F, Pass I, Courtneidge SA. The novel adaptor protein Tks4 (SH3PXD2B) is required for functional podosome formation. Mol Biol Cell 2009;20:1302. [PubMed: 19144821]
58. Courtneidge SA, Azucena EF, Pass I, Seals DF, Tesfay L. The SRC substrate Tks5, podosomes (invadopodia), and cancer cell invasion. Cold Spring Harb Symp Quant Biol 2005;70:167. [PubMed: 16869750]
59. Groemping Y, Lapouge K, Smerdon SJ, Rittinger K. Molecular basis of phosphorylation-induced activation of the NADPH oxidase. Cell 2003;113:343. [PubMed: 12732142]
60. Sumimoto H, Hata K, Mizuki K, Ito T, Kage Y, Sakaki Y, Fukumaki Y, Nakamura M, Takeshige K. Assembly and activation of the phagocyte NADPH oxidase. Specific interaction of the N-terminal Src homology 3 domain of p47phox with p22phox is required for activation of the NADPH oxidase. J Biol Chem 1996;271:22152. [PubMed: 8703027]
61. Duong LT, Rodan GA. PYK2 is an adhesion kinase in macrophages, localized in podosomes and activated by beta(2)-integrin ligation. Cell Motil Cytoskeleton 2000;47:174. [PubMed: 11056520]

62. Ambasta RK, Kumar P, Griendling KK, Schmidt HH, Busse R, Brandes RP. Direct interaction of the novel Nox proteins with p22phox is required for the formation of a functionally active NADPH oxidase. J Biol Chem 2004;279:45935. [PubMed: 15322091]

63. Ueno N, Takeya R, Miyano K, Kikuchi H, Sumimoto H. The NADPH oxidase Nox3 constitutively produces superoxide in a p22phox-dependent manner: its regulation by oxidase organizers and activators. J Biol Chem 2005;280:23328. [PubMed: 15824103]

64. Hilenski LL, Clempus RE, Quinn MT, Lambeth JD, Griendling KK. Distinct subcellular localizations of Nox1 and Nox4 in vascular smooth muscle cells. Arterioscler Thromb Vasc Biol 2004;24:677. [PubMed: 14670934]

65. Chen K, Kirber MT, Xiao H, Yang Y, Keaney JF Jr. Regulation of ROS signal transduction by NADPH oxidase 4 localization. J Cell Biol 2008;181:1129. [PubMed: 18573911]

66. Martyn KD, Frederick LM, von Loehneysen K, Dinauer MC, Knaus UG. Functional analysis of Nox4 reveals unique characteristics compared to other NADPH oxidases. Cell Signal 2006;18:69. [PubMed: 15927447]

67. Ago T, Nunoi H, Ito T, Sumimoto H. Mechanism for phosphorylation-induced activation of the phagocyte NADPH oxidase protein p47(phox). Triple replacement of serines 303, 304, and 328 with aspartates disrupts the SH3 domain-mediated intramolecular interaction in p47(phox), thereby activating the oxidase. J Biol Chem 1999;274:33644. [PubMed: 10559253]

68. Kawahara T, Ritsick D, Cheng G, Lambeth JD. Point mutations in the proline-rich region of p22phox are dominant inhibitors of Nox1- and Nox2-dependent reactive oxygen generation. J Biol Chem 2005;280:31859. [PubMed: 15994299]

69. Meng TC, Fukada T, Tonks NK. Reversible oxidation and inactivation of protein tyrosine phosphatases in vivo. Mol Cell 2002;9:387. [PubMed: 11864611]

70. Oikawa T, Itoh T, Takenawa T. Sequential signals toward podosome formation in NIH-src cells. J Cell Biol 2008;182:157. [PubMed: 18606851]

71. Cheng G, Lambeth JD. NOXO1, regulation of lipid binding, localization, and activation of Nox1 by the Phox homology (PX) domain. J Biol Chem 2004;279:4737. [PubMed: 14617635]

72. Chellaiah MA, Biswas RS, Yuen D, Alvarez UM, Hruska KA. Phosphatidylinositol 3,4,5-trisphosphate directs association of Src homology 2-containing signaling proteins with gelsolin. J Biol Chem 2001;276:47434. [PubMed: 11577104]

73. Angers-Loustau A, Cote JF, Charest A, Dowbenko D, Spencer S, Lasky LA, Tremblay ML. Protein tyrosine phosphatase-PEST regulates focal adhesion disassembly, migration, and cytokinesis in fibroblasts. J Cell Biol 1999;144:1019. [PubMed: 10085298]

74. Sastry SK, Lyons PD, Schaller MD, Burridge K. PTP-PEST controls motility through regulation of Rac1. J Cell Sci 2002;115:4305. [PubMed: 12376562]

75. Wu RF, Xu YC, Ma Z, Nwariaku FE, Sarosi GA Jr, Terada LS. Subcellular targeting of oxidants during endothelial cell migration. J Cell Biol 2005;171:893. [PubMed: 16330715]

76. Brumell JH, Burkhardt AL, Bolen JB, Grinstein S. Endogenous reactive oxygen intermediates activate tyrosine kinases in human neutrophils. J Biol Chem 1996;271:1455. [PubMed: 8576138]

77. Shono T, Yokoyama N, Uesaka T, Kuroda J, Takeya R, Yamasaki T, Amano T, Mizoguchi M, Suzuki SO, Niiro H, Miyamoto K, Akashi K, Iwaki T, Sumimoto H, Sasaki T. Enhanced expression of NADPH oxidase Nox4 in human gliomas and its roles in cell proliferation and survival. Int J Cancer 2008;123:787. [PubMed: 18508317]

78. Laurent E, McCoy JW 3rd, Macina RA, Liu W, Cheng G, Robine S, Papkoff J, Lambeth JD. Nox1 is over-expressed in human colon cancers and correlates with activating mutations in K-Ras. Int J Cancer 2008;123:100. [PubMed: 18398843]

79. Berdeaux RL, Diaz B, Kim L, Martin GS. Active Rho is localized to podosomes induced by oncogenic Src and is required for their assembly and function. J Cell Biol 2004;166:317. [PubMed: 15289494]

80. We thank Gary Bokoch and Davide Gianni for helpful discussions and suggestions, Ulla Knaus for advice and p22 reagents, Tomas Mustelin for antibodies to PTP-PEST, and Alissa Weaver for SCC61 cells. We thank Yoav Altman, Joseph Russo and Ed Monosov for help with ROS measurements. We are especially grateful to Eduardo Azucena, Paul Bromann and Marshall Peterman for their help in the early stages of this project. Research in the Courtneidge laboratory is supported by the National Cancer Institute and the Mathers Foundation.

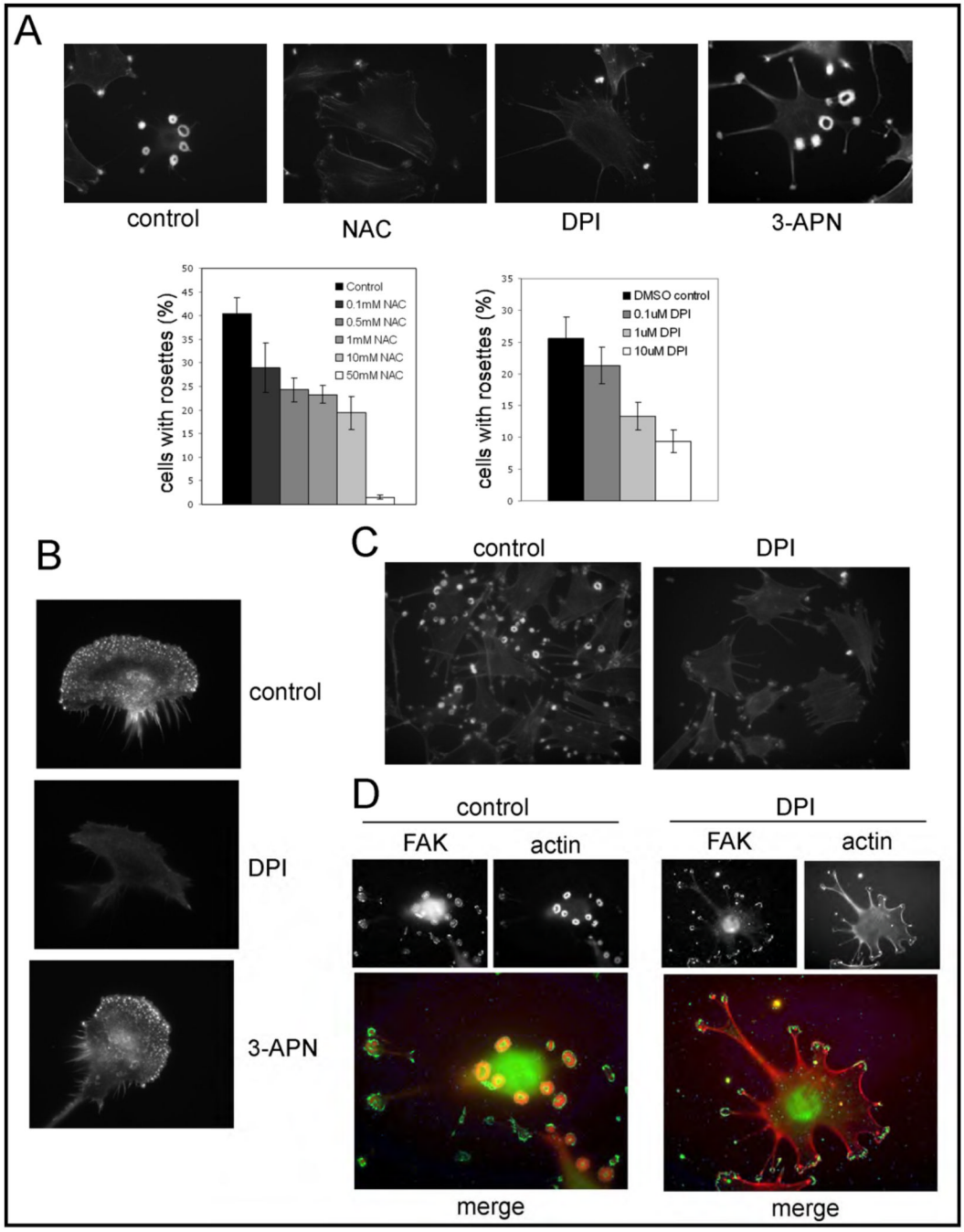


**Figure 1. ROS are required for invadopodia and podosome formation**

Panel A. NAC and DPI inhibit invadopodia formation in Src-3T3 cells.

Src-3T3 cells were plated onto coverslips, treated with vehicle (DMSO), NAC (10mM), DPI (20μM) and 3-APN (300μM), and processed for F-actin staining. Representative images (63×) are shown on the top. On the bottom, a dose response to NAC and DPI was performed and the quantitation of rosettes of invadopodia in least 150 cells per experimental point is shown.

Panel B. DPI inhibits podosome formation in macrophages.

IC-21 cells were incubated with vehicle (control, top), 20μM DPI (middle) or 300μM 3-APN (bottom) and stained with phalloidin to visualize podosomes.

Panel C. DPI reduces F-actin content.

Src-3T3 cells treated with vehicle (control, left) or 20μM DPI (right) were incubated with 0.05 U/ml phalloidin and images captured with the same exposure time.
Panel D. FAK localization is affected by DPI treatment.
Control and 20μM DPI-treated Src-3T3 cells were stained with antibodies to FAK or with phalloidin.

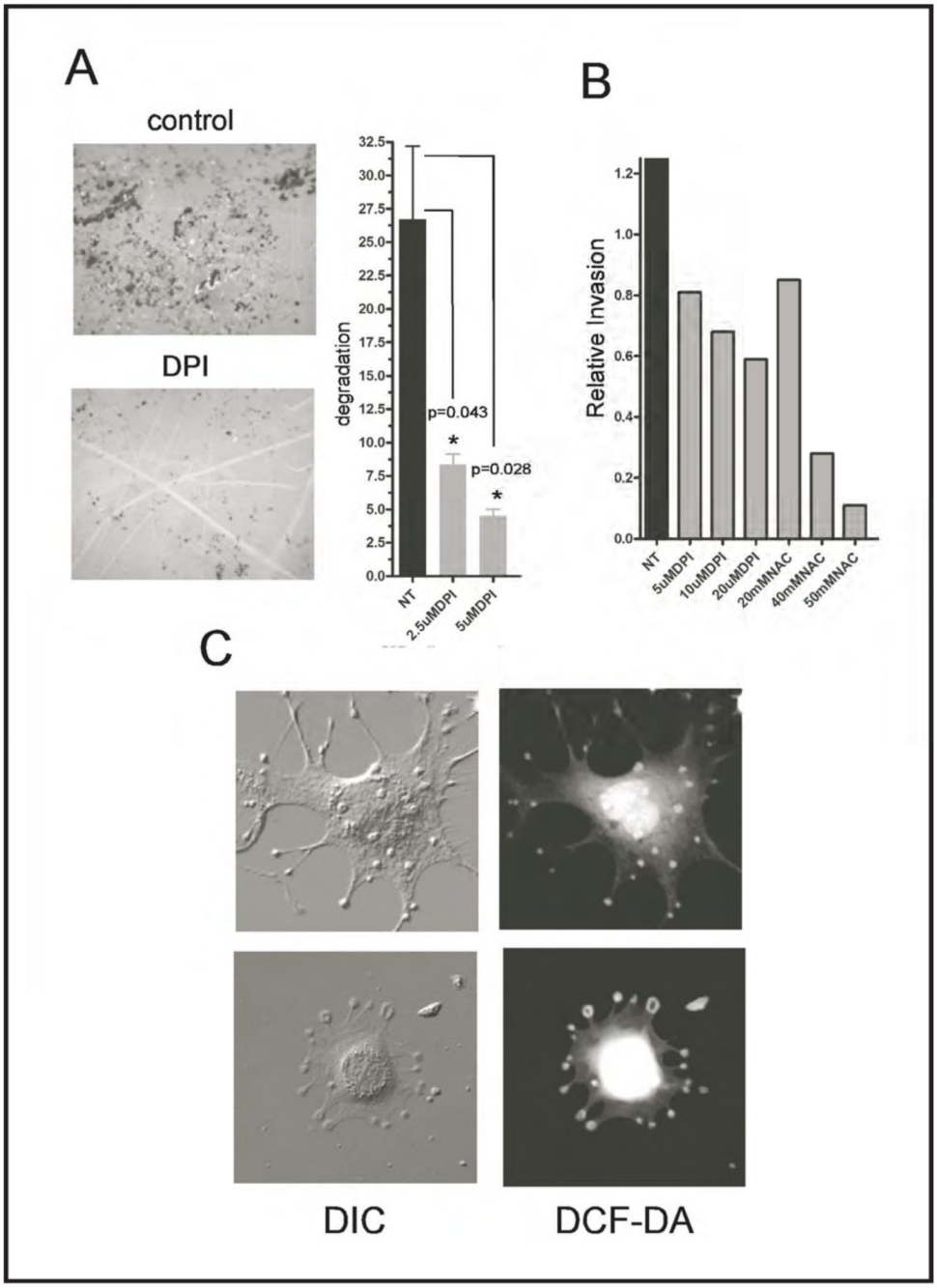


**Figure 2. ROS are required for gelatin degradation and invasion, and ROS are localized to invadopodia**

Panel A. DPI inhibits gelatin degradation.

Src-3T3 cells were plated on fluorescently labeled gelatin coated coverslips and treated with 20μM DPI 1.5h later. Cells were cultured for additional 5.5h after treatment and processed for F-actin staining. A representative image (obtained from an area containing comparable numbers of cells) of the gelatin degradation is shown on the left (40×), and the quantitation of one representative experiment from three is shown on the right.

Panel B. NAC and DPI inhibit matrigel invasion.

Src-3T3 cells were treated with the indicated inhibitors and assayed for matrigel invasion as described in Materials and Methods.

Panel C. Some ROS localize to invadopodia

Src-3T3 cells were incubated with the ROS probe CM-DCF-DA and visualized under differential interference (DIC) or fluorescence (DCF-DA) microscopy.

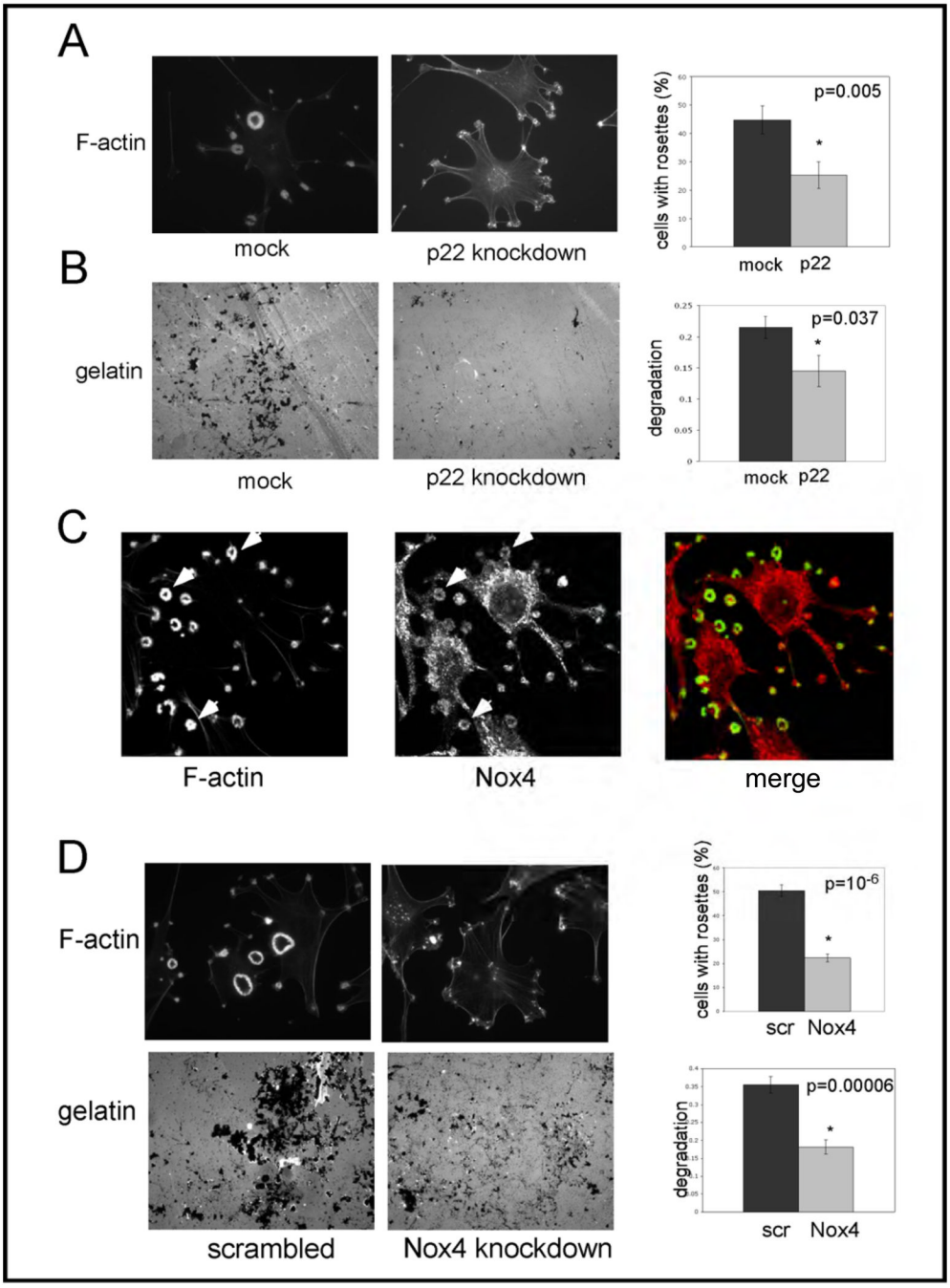


**Figure 3. The NADPH oxidase system is involved in invadopodia formation and function in Src-3T3 cells**

Panel A. Knockdown of $p22^{phox}$ reduces invadopodia number.

Src-3T3 cells were treated with transfection reagent alone (mock) or with a pool of p22phox siRNAs (p22 knockdown) and assayed for invadopodia formation. Representative images are shown on the left (F-actin staining at 63×), and quantitation of at least 150 cells per experimental point on the right. The experiment was repeated three times with similar results.

Panel B. Knockdown of $p22^{phox}$ reduces gelatin degradation.

Src-3T3 cells were treated with transfection reagent alone (mock) of a mixture of p22phox siRNAs (p22 knockdown) and assayed for gelatin degradation. Representative images obtained

at 40× from areas of similar cell density are shown on the left, and quantitation of at least 150 cells per experimental point on the right.

Panel C. Nox4 localizes to invadopodia.

Src-3T3 cells were fixed and stained with fluorescently-conjugated phalloidin (green) or with an antibody specific for Nox4 (red), and processed for confocal microscopy. Arrowheads point to rosettes showing co-localization of F-actin and Nox4. A merged image is shown on the right.

Panel D. Nox4 is required for invadopodia formation and gelatin degradation.

Src-3T3 cells were infected with lentiviruses expressing either a control (scrambled) or Nox4 shRNA (Nox4 knockdown) and assayed for invadopodia formation or gelatin degradation Representative images are shown (top, 60× for F-actin staining; bottom, 40× for labeled gelatin on areas with similar cell density). Quantitation of at least 150 cells per experimental condition are shown at the right. The experiment was repeated three times for invadopodia detection, and twice for gelatin degradation with similar results.

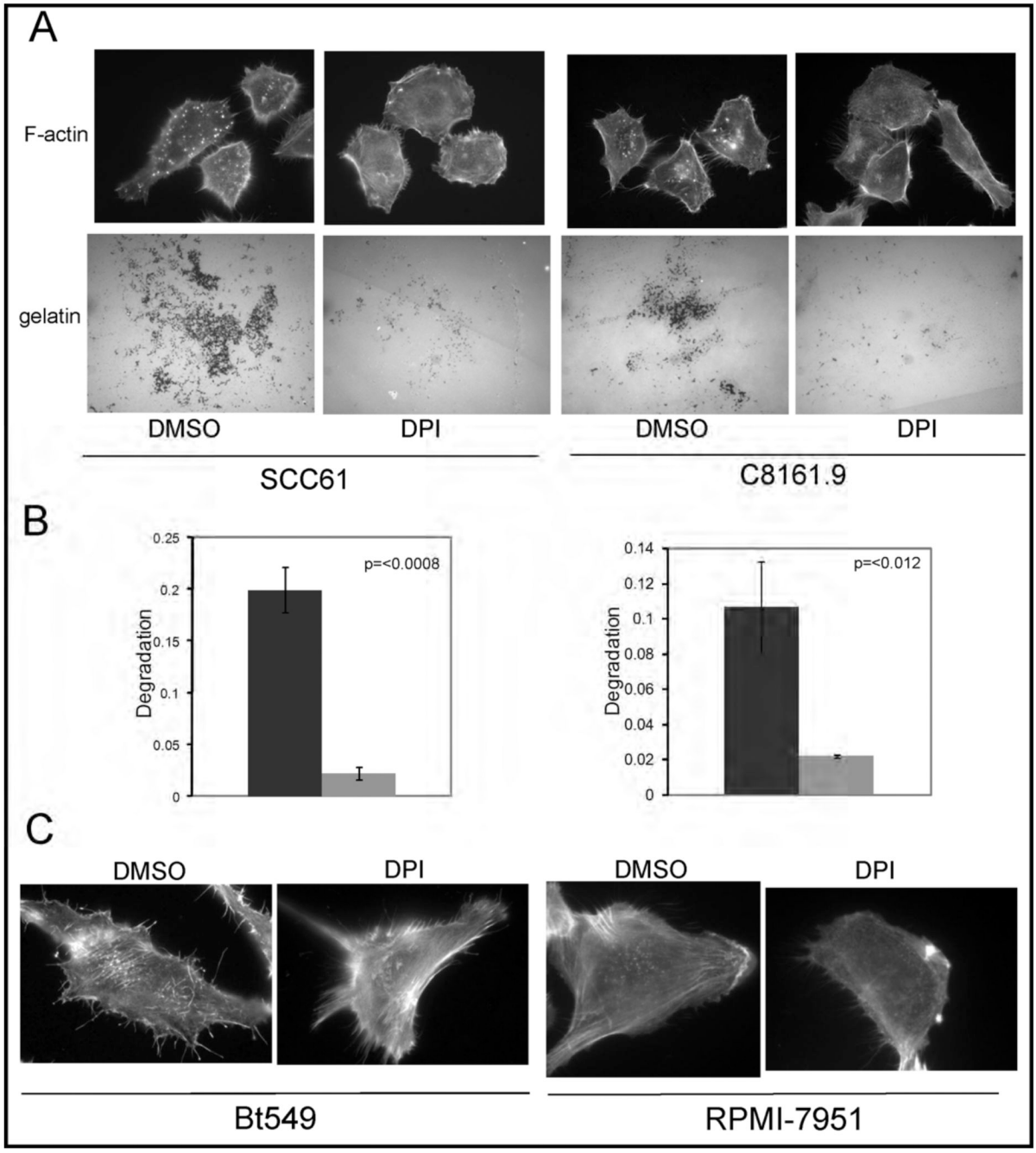


**Figure 4. Nox-generated ROS are required for invadopodia formation and function in human cancer cells**

Panel A. DPI inhibits invadopodia formation and gelatin degradation in the human cancer cell lines SCC61 and C8161.9.

Cancer cells were grown on gelatin-coated coverslips, treated with DMSO or 20μM DPI, then assayed for invadopodia formation (F-actin) and gelatin degradation (gelatin).

Panel B. Quantitation of gelatin degradation.

Quantitation of the gelatin degradation at least 50 SCC61 (left) and C8161.9 (right) cells are shown.

Panel C. DPI inhibits invadopodia formation in BT549 and RPMI-7951 cells.

Cancer cells were grown on gelatin-coated coverslips, treated with DMSO or 20μM DPI, then assayed for invadopodia formation (F-actin).

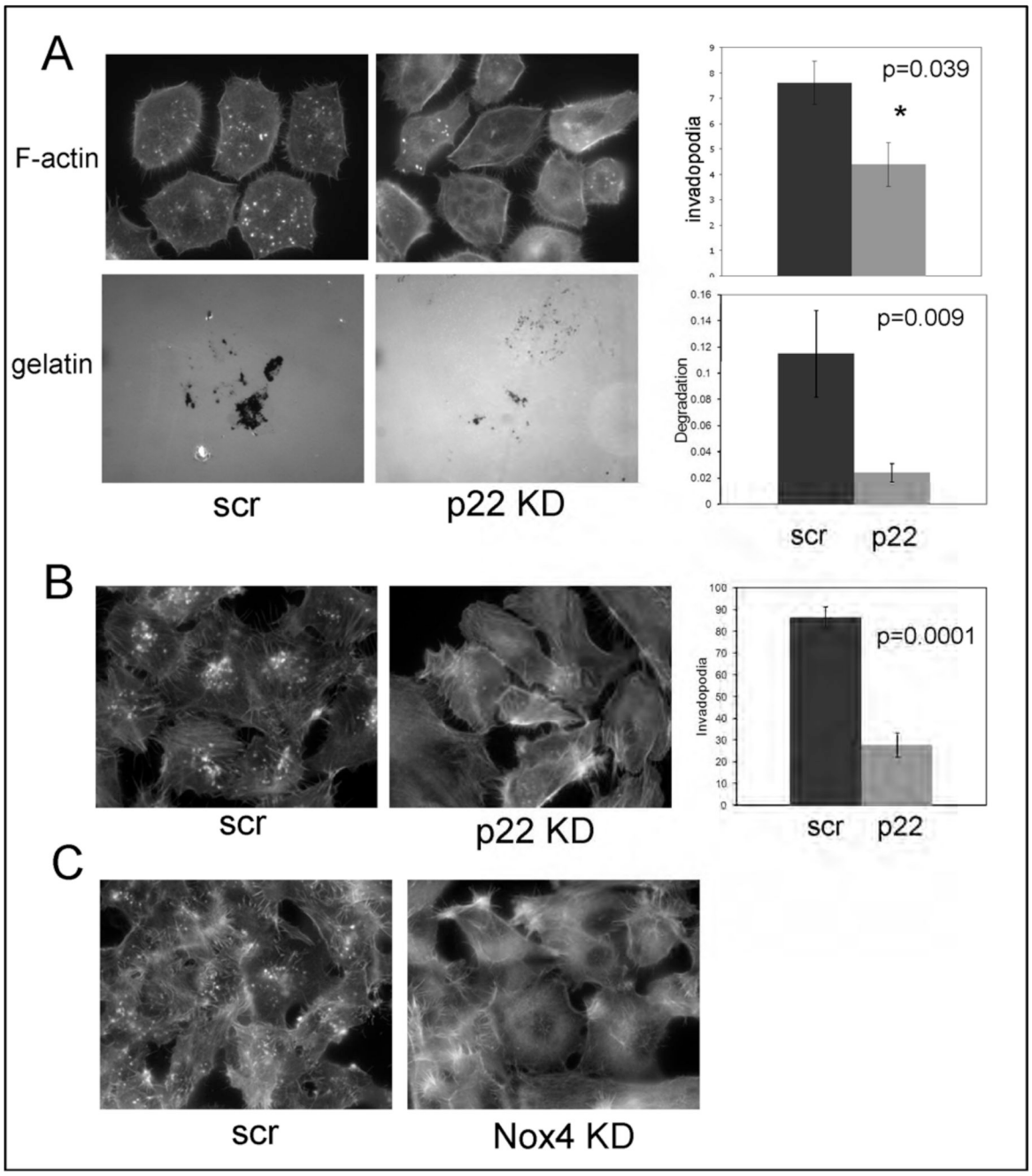


**Figure 5. NADPH oxidases are required for invadopodia formation and function**

Panel A. Knockdown of $p22^{phox}$ reduces invadopodia number and FITC-gelatin degradation in SCC61 cells.

SCC61 cells were transfected with scrambled control (scr) or a p22 siRNA (p22 KD) and assayed for invadopodia formation (F-actin) and gelatin degradation (gelatin). Representative images are shown on the left. Quantitation of at least 150 cells is shown on the right.

Panel B. Knockdown of $p22^{phox}$ reduces invadopodia number in C8161.9 cells.

C8161.9 cells were infected with scrambled control (scr) or a p22 shRNA (p22 KD) and assayed for invadopodia formation (F-actin). Representative images are shown on the left. Quantitation of at least 150 cells is shown on the right.

Panel C. Nox4 is required for invadopodia formation in C8161.9 cells.
C8161.9 cells were transfected with scrambled (scr) or Nox4-specific siRNAs and assayed for invadopodia formation. No invadopodia were detected in any Nox4 knockdown cells.

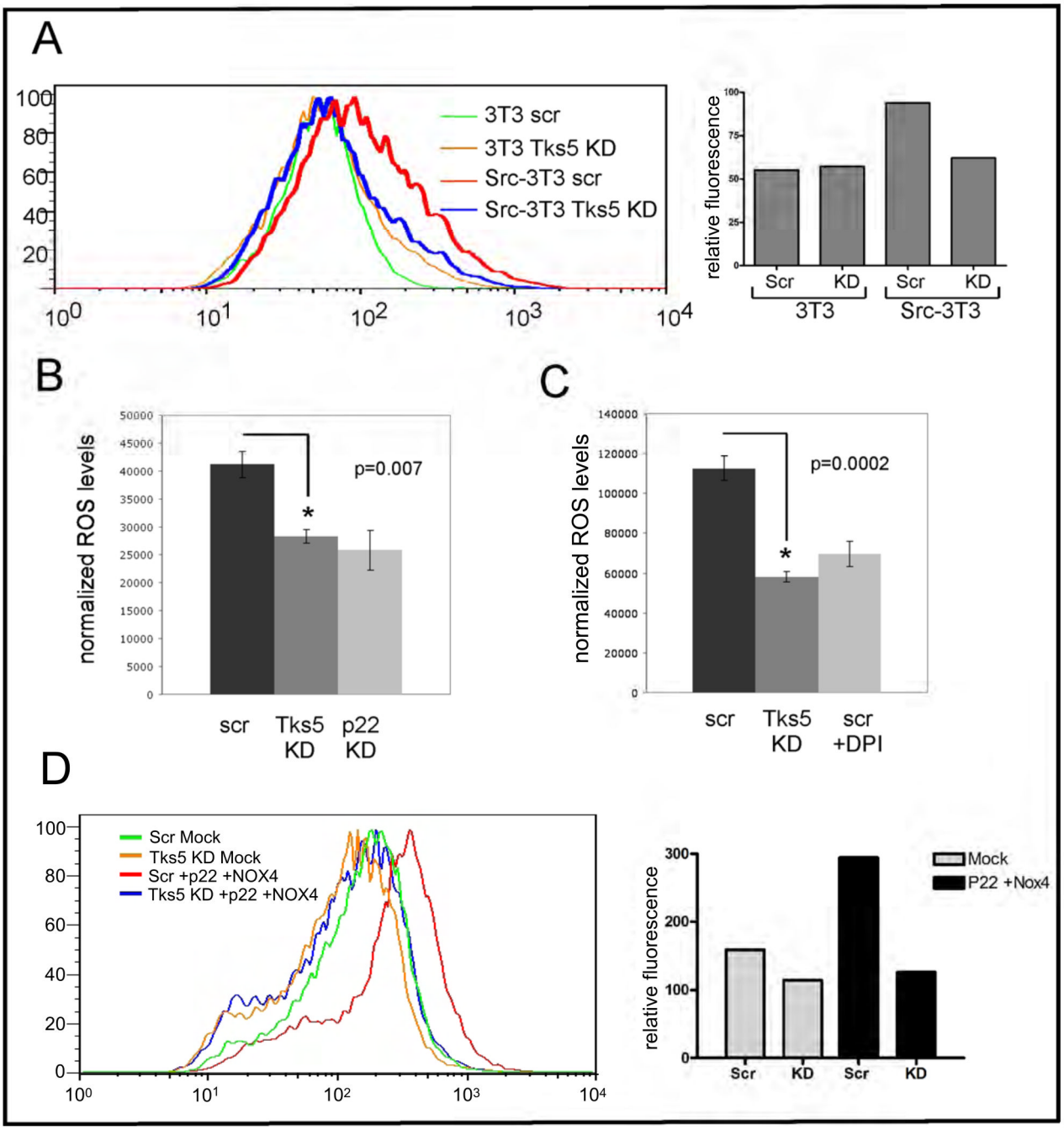


**Figure 6. Tks5 is required for ROS production**

Panel A. Tks5 knockdown reduces ROS in Src-3T3 cells as measured by DCF-DA.

3T3 and Src-3T3 cells were infected with control (Scr) or Tks5-specific shRNAs, incubated with CM-DCF-DA and analyzed on by FACS (left). ROS level quantitation is shown on the right. Knockdown of Tks5 levels is shown in Supplementary Figure 5.

Panel B. Tks5 knockdown reduces ROS levels in Src-3T3 cells as measured by luminol chemiluminescence.

Src-3T3 cells were transfected with control (scr), Tks5 (Tks5 KD) or p22phox (p22 KD) specific siRNAs, and ROS levels quantitated by a luminol-based chemoluminescence assay. Knockdown of $p22^{phox}$ and Tks5 is shown in Supplementary Figures 4 and 5 respectively.

Panel C. Tks5 knockdown reduces ROS levels in SCC61 cells as measured by luminol chemiluminescence.

SCC61 cells were transfected with control (scr) or a pool of Tks5 specific siRNAs (Tks5 KD). One hour before the assay, the control cells were incubated with either DMSO or 20μM DPI, and ROS levels were then quantitated by a luminol-based chemoluminescence assay. The degree of knockdown of Tks5 is shown in Supplementary Figure 5.

Panel D. Nox4-mediated ROS production requires Tks5.

B16-F10 melanoma cells were infected with lentiviruses expressing scrambled or Tks5-specific shRNAs, and transfected with cDNAs for Nox4 and p22 24 hours later. 48 hours after transfection cells were incubated with CM-DCF-DA and ROS levels determined by FACS. Quantitation of ROS levels is shown on the right, and analysis of Tks5, Nox4 and p22 levels in Supplementary Figure 5.

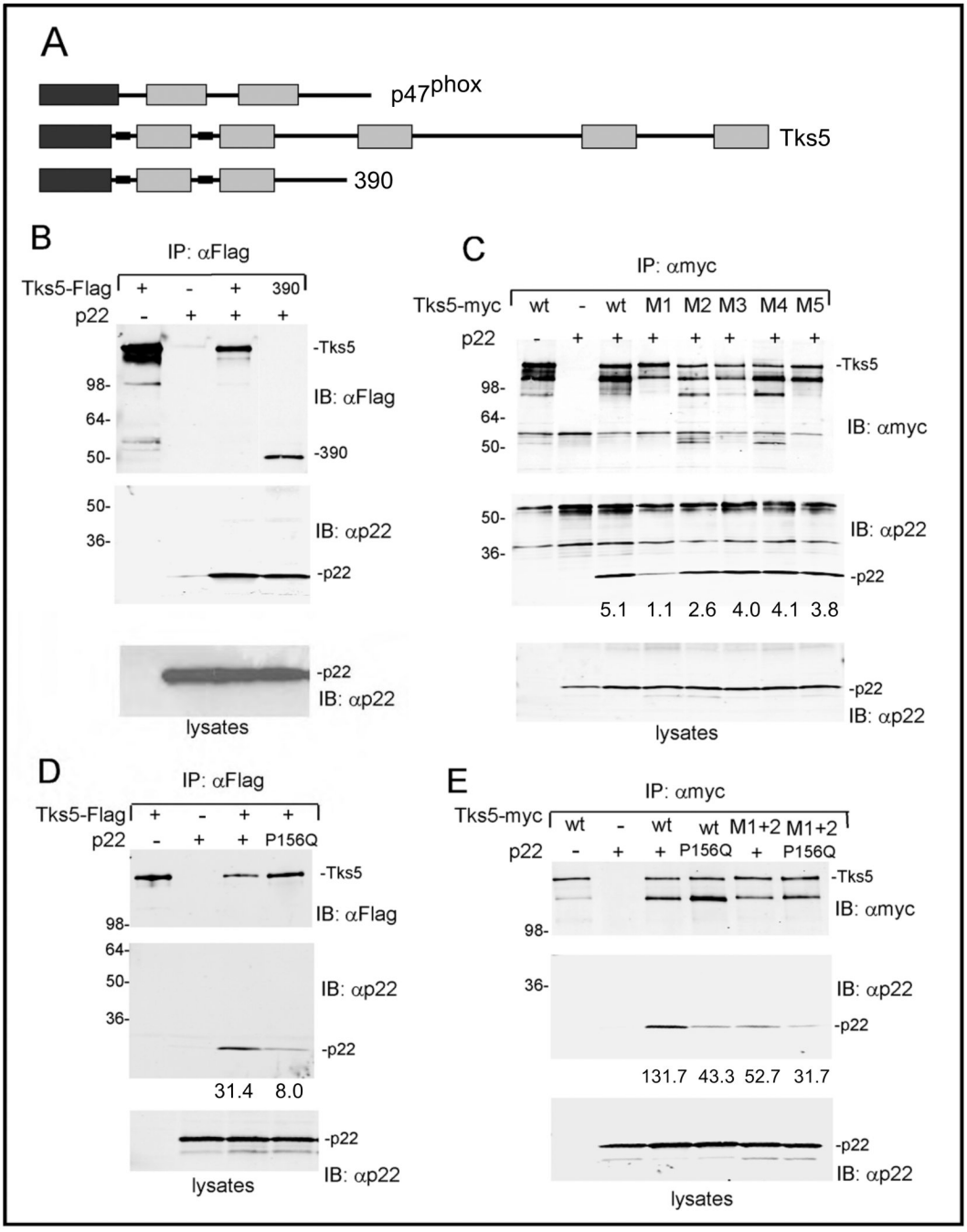


**Figure 7. Tks5 and p22$^{phox}$ can associate**

Panel A. Schematic of Tks5, p47$^{phox}$, and the Tks5 truncation mutant 390.

Panel B. Co-transfection of Tks5 and p22$^{phox}$.

293T cells were transfected with the indicated plasmids, lysed and processed for immunoprecipitation and immunoblotting with the antibodies shown. The upper panel shows the immunoprecipitation and immunoblotting of Tks5, the lower panel shows the level of p22$^{phox}$ in whole cell lysates, and the middle panel is an immunoblot of Tks5 immunoprecipitates with p22 antibody, to probe for Tks5/p22 association.

Panel C. Analysis of Tks5 mutants

Tks5 mutants containing point mutations in the ligand binding surface of each SH3 domain (M1–M5) were tested for $p22^{phox}$ association as described in panel A. The numbers at the base of the middle panel are the relative pixel density for the $p22^{phox}$ bands.

Panel D. Analysis of p22phox mutants.

Wild-type and P156Q versions of $p22^{phox}$ were tested for their ability to bind Tks5. The numbers at the base of the middle panel are the relative pixel density for the $p22^{phox}$ bands.

Panel E. Analysis of combination of Tks5 and $p22^{phox}$ mutants

The numbers at the base of the middle panel are the relative pixel density for the $p22^{phox}$ bands.

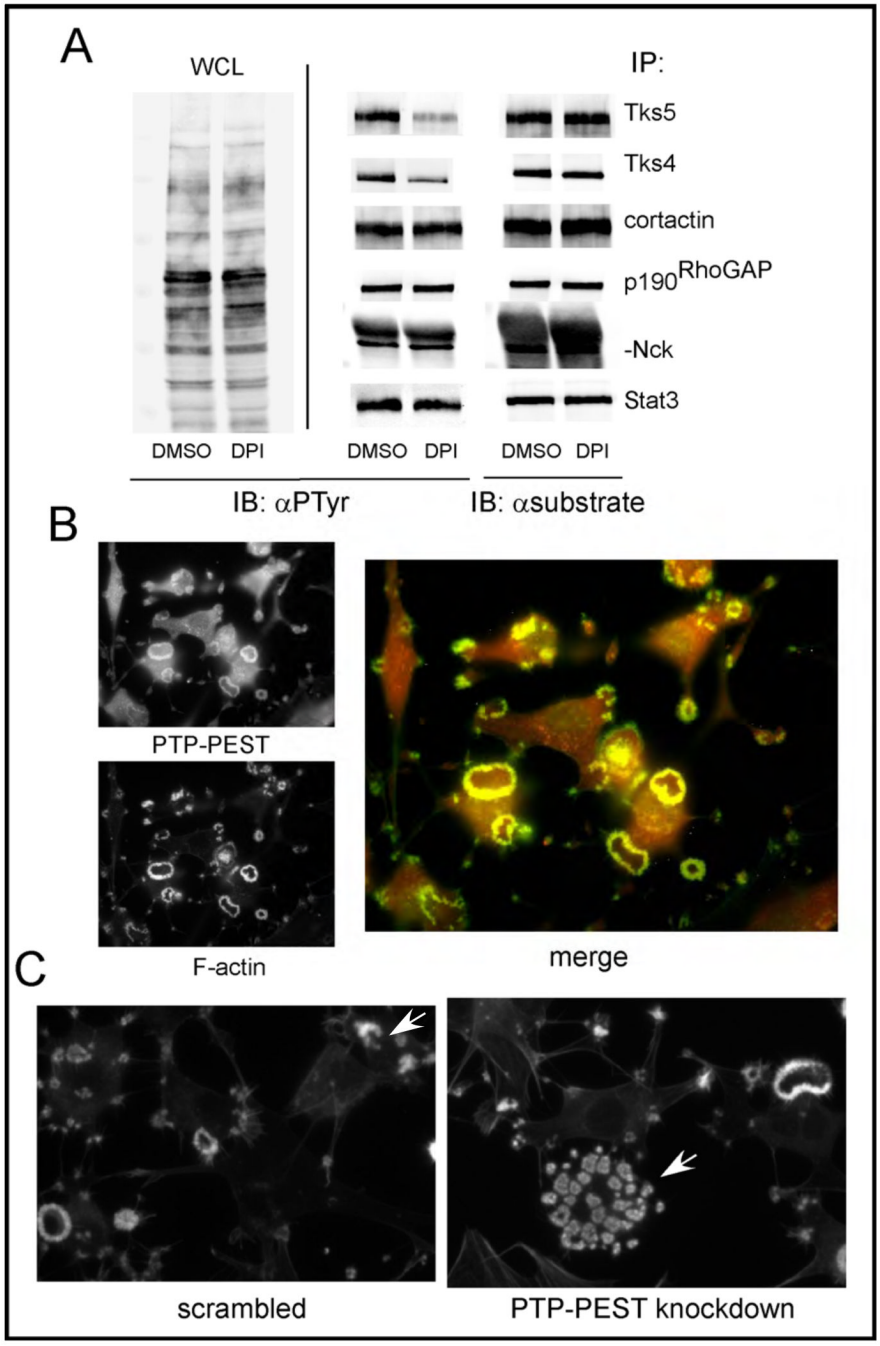


**Figure 8. ROS effects on tyrosine phosphorylation**

Panel A. Comparison of tyrosine phosphorylation levels of various Src substrates

Src-3T3 cells were incubated with DMSO or DPI, then lysed and immunoprecipitated with the antibodies shown. Immunoblotting was conducted with anti-phosphotyrosine (αPTyr) antibodies on the lysates (WCL) on the left, and the immunoprecipitates in the middle panel. On the right, each immunoprecipitate was immunoblotted with cognate antibody to control for loading. Quantification of the relative phosphotyrosine levels by densitometry is shown in Supplementary Figure 6.

Panel B. Localization of PTP-PEST to invadopodia

Src-3T3 cells were stained with phalloidin, to visualize the F-actin, and an antibody specific for PTP-PEST, and analyzed by fluorescent microscopy.

Panel C. Knockdown of PTP-PEST increases invadopodia number

Src-3T3 cells were transfected with scrambled or PTP-PEST pooled siRNAs, along with a fluorescent reporter oligo, and stained with phalloidin 72 hours later. In both cases, the arrow indicates one cell positive for the reporter oligo, in a field of otherwise reporter-negative cells.